

LASER APPLICATIONS AND OTHER TOPICS IN QUANTUM ELECTRONICS

PACS numbers: 42.62.Be; 42.55.Wd; 42.65.Re; 87.50.W–; 87.19.Pp
DOI: 10.1070/QE2012v042n03ABEH014760

Femtosecond lasers for microsurgery of cornea*

S.K. Vartapetov, D.V. Khudyakov, K.E. Lapshin, A.Z. Obidin, I.A. Shcherbakov

Abstract. **The review of femtosecond laser installations for medical applications is given and a new femtosecond ophthalmologic system for creation of a flap of corneal tissue during the LASIK operation is described. An all-fibre femtosecond laser emitting ~400-fs pulses at 1067 nm is used. The pulse repetition rate can vary from 200 kHz up to 1 MHz. The output energy of the femtosecond system does not exceed 1 μJ. A specially developed objective with small spherical and chromatic aberrations is applied to focus laser radiation to an area of an eye cornea. The size of the focusing spot does not exceed 3 μm. To process the required area, scanning by a laser beam is applied with a speed no less than 5 m s^{-1}. At a stage of preliminary tests of the system, the K8 glass, organic PMMA glass and specially prepared agarose gels are used as a phantom of an eye. The femtosecond system is successfully clinically tested on a plenty of eyes of a pig and on several human eyes. The duration of the procedure of creation of a corneal flap does not exceed 20 s.**

Keywords: *ophthalmologic laser system, LASIK, femtosecond fibre laser, femtosecond laser pulse–tissue interaction, photodisruption, single-wall carbon nanotubes.*

1. Introduction

Ultrashort laser pulses allow high laser intensity to be reached at very low pulse energies. Photodisruption of transparent media can result from focusing a laser beam into the bulk of transparent media [1], the thermal effects being low due to the short pulse duration. Tissue processing with femtosecond laser pulses has been of growing interest since its high precision was demonstrated on a variety of different tissues. Moreover, due to its submicrometre precision, it is possible to perform such surgical procedures as refractive surgery inside the human eye. Many studies have been performed to compare the efficiency of femtosecond lasers and mechanical microkeratomes for corneal flap creation in laser *in situ* keratomileusis (LASIK) [2]. At present there are only several companies which produce femtosecond lasers for flap creation. Many of these companies use bulk solid-state femtosecond lasers, which generate ultrashort pulses; however, these lasers are very sensitive to environmental fluctuations. Therefore, frequent adjustment of the laser cavity is necessary, which complicates the maintenance procedure.

Since it is necessary in actual laser surgeries to have energy values greater than the threshold, we need to use the shortest possible pulse duration to introduce the lowest amount of energy into the cornea. It is known that the intensity I of a light pulse with time duration of a few hundreds of femtoseconds is sufficient to exceed the corneal photodisruption threshold [3]. Femtosecond fibre lasers can generate pulses with duration less than 100 fs and offer more environmental stability in comparison with bulk solid-state lasers. Moreover, the femtosecond fibre lasers do not need frequent maintenance and are easily integrated into medical devices. Thus, a fibre femtosecond laser, as a stable and reliable source, is a preferable laser for application in eye surgery.

Recently, nonlinear optical properties of single-wall carbon nanotubes (SWNTs) have been widely used in optical devices to control laser irradiation. Applications of SWNT-based saturable absorbers for passive mode-locking spread over a wide range of wavelengths from 1 to 1.99 μm in fibre and bulk solid-state laser systems. Such a spectral band of SWNT application is determined by optical properties of the nanotubes, because the absorption spectrum of semiconductor SWNTs has most intensive transitions E_{22s} and E_{11s} near 1.1 and 1.6 μm, respectively [4–9]. The spectral position of the absorption bands is a function of the nanotube's diameter and, therefore, depends on the method of synthesis.

Using the dependence of spectral properties of the nanotubes on their diameter [10], it is possible to select a range of diameters of the SWNTs extracted as a result of their synthesis and further purification so that one of the absorption bands lies in the vicinity of the operating wavelength, which increases the modulation depth of saturable absorption. In our case, if lasing occurs near $\lambda = 1.06$ μm, we have to use nanotubes with diameters 0.95–1.1 nm when the centre of the transitions E_{22s} is near $\lambda = 1$ μm. Such synthesis processes as laser ablation with a RhPd catalyst and high-pressure carbon monoxide (HiPCO) process with a Fe or Co–Mo catalyst can ensure the desired distribution of diameters of the nanotubes [11, 12]. SWNT-based saturable absorbers can easily be prepared as thin polymer films which makes them promising as compared with semiconductor saturable absorber mirrors (SESAMs) that require complex and expensive fabrication techniques [13]. Operation of a 1.55-μm pulsed fibre laser

*Reported at XIX International Conference on Advanced Laser Technologies (ALT'11), Bulgaria, Golden Sands, September 2011.

S.K. Vartapetov, K.E. Lapshin, A.Z. Obidin Physics Instrumentation Center at A.M. Prokhorov General Physics Institute, Russian Academy of Sciences, ul. Tsentral'naya 1, 142190 Troitsk, Russia; e-mail: svart@pic.troitsk.ru;
D.V. Khudyakov Optosystems Ltd., Physics Instrumentation Center at A.M. Prokhorov General Physics Institute, Russian Academy of Sciences, ul. Tsentral'naya 1, 142190 Troitsk, Russia;
I.A. Shcherbakov A.M. Prokhorov General Physics Institute, Russian Academy of Sciences, ul. Vavilova 38, 119991 Moscow, Russia

Received 28 October 2011
Kvantovaya Elektronika **42** (3) 262–268 (2012)
Translated by D.V. Khudyakov

with a polymer composite SWNT with carboxymethylcellulose (CMC) as a saturable absorber was successfully demonstrated in [14].

This paper describes a new femtosecond laser system for ophthalmology, which is used as bladeless microkeratome for flap creation. The paper also reports the model of a femtosecond all-normal dispersion fibre laser with a SWNT-CMC thin-film saturable absorber for passive mode-locking at λ = 1067 nm.

2. Analysis of parameters of femtosecond systems

Currently available femtosecond laser systems for ophthalmology usually use two basic paradigms in the photodisruptive process. One employs high-energy (several μJ) pulses and relatively low pulse repetition rates (5–60 kHz). The other applies low-energy (hundreds of nJ), high-frequency (1–80 MHz) pulses. It is obvious that the different paradigms require dissimilar beam scanning algorithms because due to specificity of physical processes taking place in them, the processing results strongly depend both on the spatial position of the laser beam spot and on the sequence of irradiation (cumulative effect of plasma formation) of the tissue region. Higher-energy pulses allow greater spacing between the spots, because the expanding gas bubbles, much exceeding the size of the laser action, drive the cutting process. But wide spacing can result in uncut areas or bridges of the tissue. While lower-energy pulses and smaller spot sizes require the use of more spots placed substantially closer together, because the cumulative effect for plasma formation is the primary driver of the tissue cutting process. Comprehensive analysis of commercially available femtosecond platforms for refractive surgery is given in paper [15].

Parameters of the ophthalmology system have great influence on the laser radiation – tissue interaction processes. Besides, they should satisfy certain customer requirements. Thus, the pulse duration τ should comply with a minimal photodisruption threshold. The pulse energy E should be optimal to comply with the smallest disruption volume of a cornea. The spot size d should be as small as possible for given conditions to ensure high treatment quality. The laser wavelength λ should meet several requirements. On the one hand, a wavelength near maximal transparency of a cornea should be chosen, and on the other hand, retinal sensitivity should be minimal at the chosen wavelength. In addition it is desirable that the wavelength would be available from widely used laser media and a highly efficient apparatus. The repetition rate should be high enough to provide minimal duration of the medical procedure. In particular, to treat a surface of diameter 10 mm for t =15 s with $d \sim 2$–3 μm and the spot spacing 2–3 μm, it is necessary to produce $\sim 10^7$ laser pulses, i.e., the required pulse repetition rate f should amount to ~1 MHz.

A more detailed analysis of the parameters of now available femtosecond ophthalmology systems makes it possible to determine a set of general requirements for engineering development of femtosecond devices used to create a flap of cornea tissue, namely:

(i) minimum cutting thickness inside the cornea (1–3 μm);

(ii) large scan area (10 × 10 mm);

(iii) precision of treatment (~5 μm resolution);

(iv) small time of operation (less than 30 s);

(v) multistage testing and control of all parameters of the system.

3. Preliminary experiments

The subject of a separate study in this paper is the choice of the laser beam pulse energy and volume of the laser spot. The matter is that the size of the photodisruption region inside a cornea is dramatically greater than focusing spot size which we can predict by simple evaluation. Moreover, it strongly depends on the pulse energy and focusing lens parameters. As a rule, the photodisruption region has an elongate structure along the optical axis direction, thereby resembling a filament. This phenomenon is often explained by laser beam self-focusing. However, this explanation is not an only reason for filamentation.

The authors of papers [16, 17] investigated laser induced optical breakdown (LIOB) and other accompanied phenomena both in water and fused silica, which are widely used as perfect materials for eye tissue – laser irradiation interaction modelling. These papers studied the dynamics of self-focusing (SF) and LIOB processes and paid special attention to their competition. They clarified the conditions for the formation of SF and LIOB and investigated the physical mechanisms, which lead to photodisruption. Figure 1 presents one of the results of paper [16], i.e., experimental dependences of the LIOB and filamentation thresholds (filament structures where the main energy of the laser beam is concentrated) on the focal length of the objective. First of all, special attention should be given to most interesting phenomenon in Fig 1, showing some region where coexistence of filamentation and breakdown is observed under tight focusing conditions. It is this region where simultaneous emergence of two phenomena is possible: optical breakdown and self-focusing. Apparently, such a situation is absolutely impermissible in case of eye cornea treatment because in addition to photodisruption of cornea (volume of 1 μm^3), it leads to formation of long filaments which can reach the external cornea surface. Also the authors in [16] showed that in the case of self-focusing, with increasing the laser power the filament extends along the optical axis in the reverse direction from the geometrical focus of the objective when the input pulse power exceeds the critical power, given by:

$$P_{cr} = \frac{3.77\lambda^2}{8\pi n_0 n_2},$$

where λ is the laser wavelength, and n_0 and n_2 are the initial refractive index and its nonlinear increment, respectively, (n =

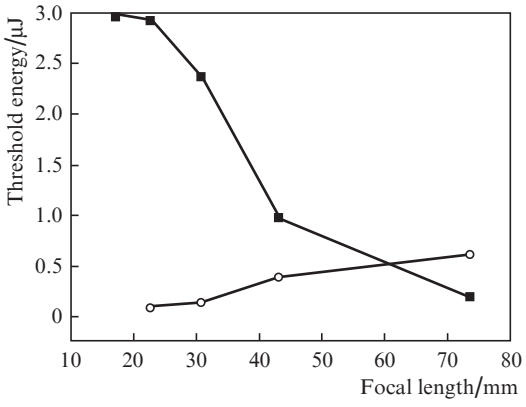

Figure 1. Threshold energies for LIOB (○) and filamentation (■) as a function of focal length.

$n_0 + n_2 I$). As follows from the above, the focusing objectives with focal distance $F > 35–40$ mm cannot be recommended for application in femtosecond ophthalmology systems. Besides, we should pay attention to a very important feature. When we use a focusing objective with short focal distance ($F < 20$ mm in Fig. 1), it is possible to achieve LIOB even by using a very small pulse energy (several tens of nJ, $\tau < 50$ fs) and produce photodisruption in a very small volume of about ~ 1 μm^3. However, one needs to use optical systems with a high numerical aperture (NA) in order to obtain a submicron laser spot size. Thus, spherical aberrations induced at the air – cornea interface should be taken into account.

To select an optimal focusing lens design and the laser pulse parameters for obtaining the minimal photodisruption volume, we performed a number of experiments on interaction of femtosecond pulses with a PMMA sample by using high NA focusing objectives. The results of these experiments are shown in Fig. 2. One can see that the length of photodestruction strongly depends on the laser pulse energy and at an optimal energy can produce small photodisruption no longer than 3 μm (Fig. 2d). Figure 3 illustrates the possibility of controlling the length of filaments by diaphragming the laser beam. By changing the laser beam diameter, we can control the value of spherical aberrations which leads to corresponding changes in the length of the destruction area. An explanation of the obtained results is given in Fig. 4. When use is made of large numerical apertures, trajectories of peripheral laser rays have different paths in the bulk of the tissue than those of the axial rays. As a result, a structure extended along the optical axis is formed. The length of such a structure is determined by the equation

$$L_f = \frac{F_d}{n}\left(\sqrt{\frac{n^2 - \sin^2\theta}{1 - \sin^2\theta}} - n\right), \qquad (1)$$

where $F_d = nF$ is the focal length in air; θ is the maximal angle of inclination of a peripheral ray to the optical axis.

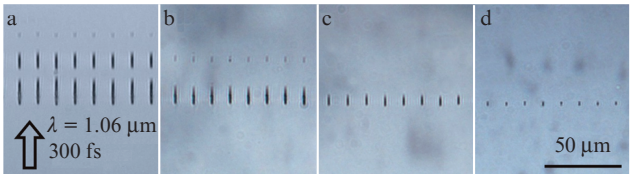

Figure 2. Length of photodisruption in a PMMA sample at a laser pulse energy of (a) 3 μJ, (b) 2.1 μJ, (c) 800 nJ, (d) 300 nJ. The focusing depth is 1 mm, the repetition rate is 50 Hz, and the numerical aperture of the focusing lens is NA = 0.5.

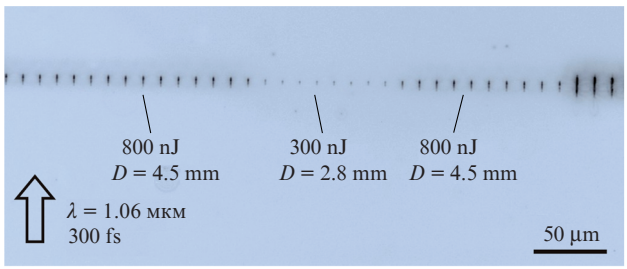

Figure 3. Control of the photodisruption length by laser beam diaphragming (D is the diameter of the diaphragm).

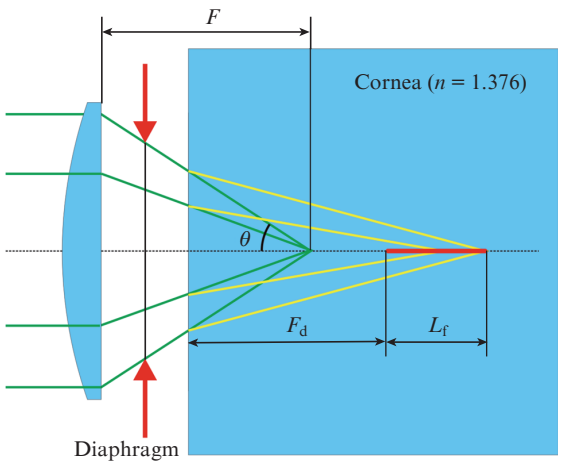

Figure 4. A schematic of focusing of the laser beams across the air – tissue interface. F_d is the geometrical focus in cornea and L_f is the foci range.

Indeed, the authors of paper [18], who studied elongation of the plasma luminescence region, observed a similar effect upon irradiation of a fused silica sample by femtosecond laser pulses under deep focusing of the laser beam by wide-aperture objectives. However, in our work the mentioned effect determined the length of photodisruption tracks produced by a femtosecond laser pulse in the PMMA sample. We assumed that the nature of these phenomena is the same. The authors of paper [18] clearly proved that the length of the plasma luminescence region is related to the numerical aperture by equation (1). In our experiments, the dependence of the length of filaments on the input pulse energy can be explained by the fact that when we increase the pulse energy of a Gaussian beam, the intensity of peripheral rays starts exceeding the level of the photodisruption threshold for a given material, and the length of the filament increases (without taking into account chromatic aberration). Thus, if we decrease the pulse energy, the material is irradiated by paraxial rays only, which leads to a decrease in the length of the filaments.

4. Apparatus description

In the system designed we used a laser emitting <400-fs pulses with a high repetition rate (~ 1 MHz) and a low energy (~ 1 μJ). The total number of laser pulses was determined by the duration of operation, which is limited to 30 seconds, and by the pulse repetition rate. The distance between laser focusing spots was 3 – 5 μm and the main goal was to spread with high uniformity the laser spots over the entire region to be treated. In accordance with the aforesaid conditions the scanning velocity of the laser beam on a target should be 3 – 5 m s^{-1}.

The high velocity of the laser beam scanning was provided by angle scanning of the mirror which deflects the laser beam to a small angle ($\sim 1°$) from the optical axis. The mirror was driven by a 10-kHz resonant galvanoscanner (GSI), which provided the corresponding scanning aberrationless field from 100 to 200 μm. The focusing objective was moved at a translation speed of 100 mm s^{-1} in the orthogonal direction to the angle scanning direction in order to treat an area of diameter 10 mm during $t < 15$ s. The focusing objective was consequently moved during scanning along a 'raster' trajectory, thereby producing scan tracks of width 200 μm (Fig. 5a) with

a distance of 100–150 μm between the tracks. The adjacent tracks overlapped. As a result, the regions were obtained where the tracks overlap two or three times (see Fig. 5b). Thus, a more uniform distribution of laser spots and as a result, a high quality of laser cutting were ensured. One can see from Fig. 5 that laser spot size at the focal point was less than 2 μm. In order to achieve such a result, a special optical system was calculated and designed which included a beam expander and a focusing objective.

The above-mentioned longitudinal spherical aberrations arising upon focusing of a laser beam through the air – tissue

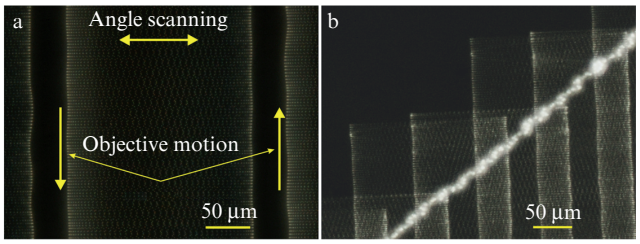

Figure 5. Optical breakdown traces produced by the femtosecond laser in the bulk of glass samples: (a) scan tracks without overlapping; (b) scan tracks with overlapping. The lens translation speed is 100 mm s^{-1}, the angle scanning velocity is 5 m s^{-1}. The image was obtained with a Nikon LV-100D microscope having a 200× magnification.

interface can be compensated for by inserting a simple spherical lens which introduces negative spherical aberrations into the laser beam. In calculating a special 4-lens microobjective, we managed not only to compensate for spherical and chromatic aberrations for the scanning field of size 200 μm but also to adjust the focal distance of the objective in range 400 μm with longitudinal aberrations less than 3 μm. A very important feature of the design consisted in the fact that the focal distance was changed by moving only one spherical lens. Such a variation in the focal distance was needed to make a vertical side cut during the corneal flap creation procedure. Besides, the objective proved very useful in other ophthalmology surgeries such as keratoplasty, keratoconus, glaucoma, where a change in the depth of laser cutting is required. The numerical aperture of the focusing objective (NA ~ 0.3) was chosen to satisfy the competition between two conditions: a small spot size required a high NA, but spherical aberrations induced at the air – cornea interface required a small NA, because aberrations grow dramatically at high numerical apertures (see Fig. 4).

For the microobjective used it was necessary to use a high quality laser beam with the input diameter ~20 mm. Because the output laser beam from the femtosecond laser had diameter ~4 mm and divergence ~2 mrad, we employed a high quality beam expander (magnification 4.2) with a diffraction limited output beam to meet focusing objective input requirements. In addition, the beam expander was used as an optical projection system between a 'fast' resonant scanner and the objective. The beam expander is mounted in such a manner that inside it the telecentric path of rays is implemented. In this case, the system ensured incidence of the laser beam into the focusing objective aperture at all working angles of the 'fast' scanning mirror.

The above-described high quality optical assemblies were used to build a fully functional 'Femto Vizum' ophthalmology system for corneal flap creation. During laboratory tests we used PMMA, silica glass and agarose gel as a cornea tissue phantom. The result of treatment of a glass sample using the algorithm providing the greatest possible uniformity of processing is shown in Fig. 6. One can see that the area of processing consists of two zones with different distributions of laser spots. The focusing objective has the translation speed 100 mm s^{-1} in the central zone. At the edge of the treatment zone the translation speed decreases to 30 mm s^{-1} to ensure more stable side cutting of the corneal flap. Figure 7 presents the exterior appearance of the femtosecond 'Femto Vizum' ophthalmology system. Clinical tests were successfully performed using our femtosecond laser system. The tests were carried out using both eyes of a pig and human eyes. Therefore, the main idea and parameters of the femtosecond laser were fully confirmed.

It is clear that the main part of the ophthalmological system is the femtosecond laser with the desired parameters. We

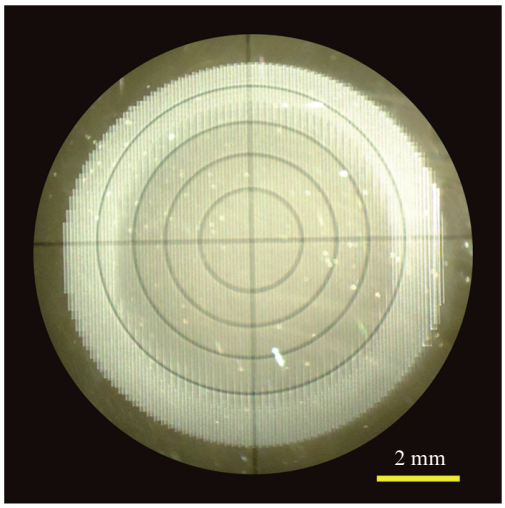

Figure 6. View of an eye phantom (glass sample) treated with the double speed technique ensuring two zones with different laser spot distributions. The image was obtained with a Leica MS5 microscope having a 40× magnification.

Figure 7. Exterior view of the femtosecond 'Femto Vizum' ophthalmology system.

used an all-fibre femtosecond laser in our 'Femto Vizum' system. In the preliminary experiments we found the basic parameters of the femtosecond laser, required for successful treatment (the spectral bandwidth less than 15 nm, pulse duration less than 400 fs, the repetition rate of 1 MHz, the nominal energy of ~2 μJ). For ophthalmological 'Femto Vizum' system we designed an all-fibre femtosecond laser.

5. All-fibre femtosecond laser

The master oscillator of the femtosecond fibre laser consisted of an active fibre segment (fabricated at IRE-Polus, Fryazino) and passive fibre segments which were built in a ring type cavity (Fig. 8). All elements of the ring cavity had normal group velocity dispersion. To provide for a stable polarisation state, the polarisation maintaining single-mode PANDA fibres (core diameter of 6 μm and clad diameter of 125 μm) were used. The active Yb-doped fibre had a length of 2.7 m and was pumped by radiation of a 960-nm laser diode with an average power up to 3W. A fibre-type polarisation-dependent isolator was inserted in the laser cavity to provide unidirectional and linear polarised modes in the cavity. The laser output coupler efficiency was 20%.

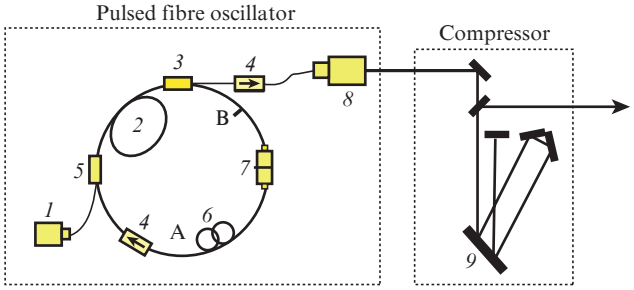

Figure 8. Scheme of the pulsed fibre oscillator and compressor: (*1*) pump laser diode; (*2*) Yb-doped fibre; (*3*) 80/20 output coupler; (*4*) fibre isolator-polariser; (*5*) 980/1060 fibre coupler; (*6*) polarisation controller; (*7*) saturation absorber with SWNTs; (*8*) fibre collimator; (*9*) diffraction grating.

To ensure self-starting and passive mode-locking in the laser, the film saturable absorber of a special design (based on a polymer composite with SWNTs) integrated into an optical fibre was used. Nonlinear optical absorption of SWNTs in a CMC thin polymer film was studied by the Z-scan method using a 400-fs probe pulse. The values of the sample saturation intensity I_s = 51 MW cm^{-2} and nonlinear absorption coefficient $\beta = -5 \times 10^{-7}$ cm W^{-1} were registered at λ = 1060 nm. The absolute value of the nonlinear absorption coefficient is comparable or even higher than that for other known nanostructures (nanocrystals SiO_2, CdS, etc.) which makes polymer composites with SWNTs a potential nonlinear optical material [19].

To prevent optical damage of the film composite SWNT-CMC, it was positioned on a side-polished fibre (Fig. 9). The distance h from the polished surface to the fibre core is an important parameter determining the transmission power and the strength of interaction with the composite film. The 10-μm-thick polymer film was placed on the surface of the side-polished fibre with the interaction length L = 5 mm and distance to core h = 1–3 μm. Such an arrangement of the composite film increases optical stability of the modulator and maintains the stable mode-locking for a long operation time. The only fibre segment between A and B points, including polarisation controller and saturable absorber, was made of an ordinary (nonpolarisation maintaining) single-mode fibre to provide for additional mode-locking because of nonlinear polarisation evolution.

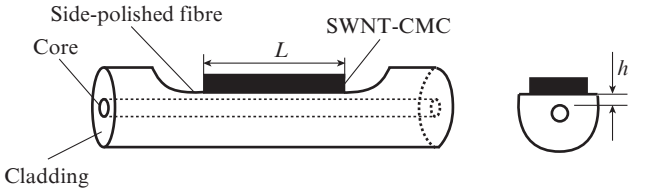

Figure 9. Schematic diagram of positioning of the composite polymer film with SWNTs on a side-polished fibre surface.

Stable mode-locked operation was observed at an average output power of 160 mW with a central lasing wavelength at 1067 nm. The all-normal dispersion fibre oscillator generated strongly chirped pulses with 16.7-MHz repetition rate corresponding to a cavity length of 12.3 m. The energy of a single pulse based on the average power of pulses and rate of their repetition was 10 nJ. The output pulse train is presented in Fig. 10. To precisely determine the single-pulse duration, we used an intensity autocorrelator with a nonlinear crystal for noncollinear second harmonic generation. The time duration of a single pulse measured directly after the oscillator was 12 ps. The pulses were dechirped by the grating compressor to get the minimal pulse duration. Figure 11a shows the autocorrelation function of a single pulse after the compressor. The full-width at half-maximum of the pulse autocorrelation function measured after the compressor was 200 fs, which corresponds to a 140-fs pulse. The output optical spectrum of the mode-locked laser shown in Fig. 11b had a spectral full-width at half-maximum of 15 nm, which corresponds to a time-bandwidth product of $\Delta\tau\Delta\nu = 0.55$, where $\Delta\tau$ is the pulse duration in seconds and $\Delta\nu$ is spectral width in reverse seconds. This value is close to theoretical time-bandwidth product $\Delta\tau\Delta\nu = 0.44$ for a transform-limited Gaussian pulse.

To increase the pulse energy up to the required level, the output pulse from the oscillator passed through a preamplifier followed by an acousto-optic pulse discriminator and a high-power amplifier. The preamplifier stage comprises ~0.5-m-long Yb-doped single-mode fibre which was pumped

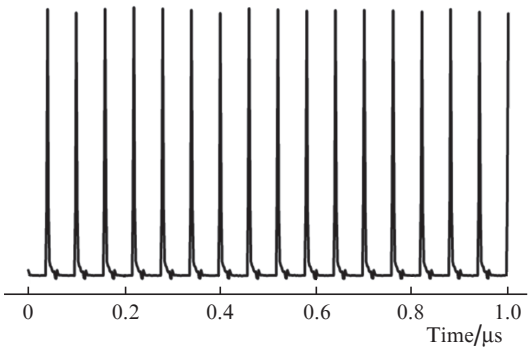

Figure 10. Pulse train at the output of the fibre oscillator.

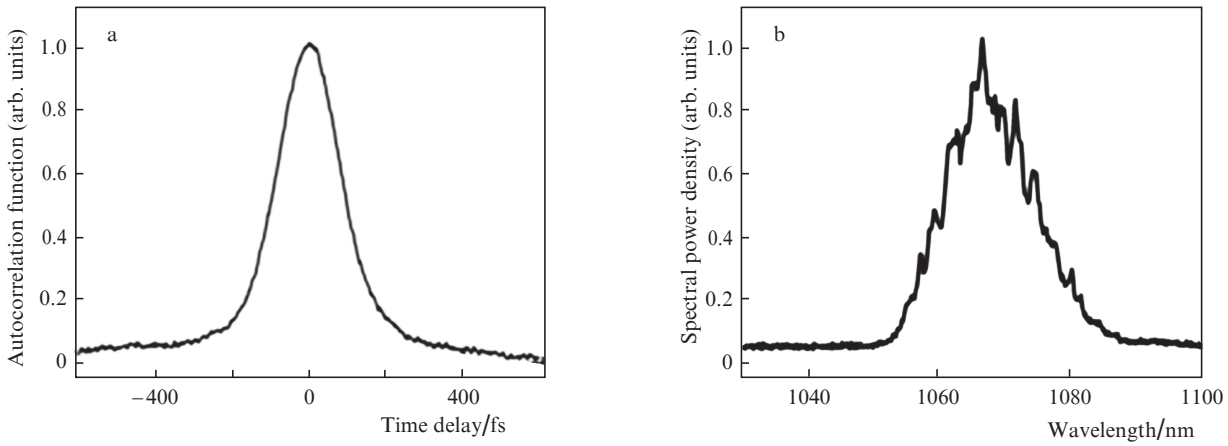

Figure 11. The output characteristics of the pulsed fibre oscillator: (a) pulse autocorrelation function after the compressor; (b) output spectrum at the output of the fibre oscillator.

by radiation of a 976-nm laser diode. The acousto-optic modulator decreased the pulse repetition rate down to the 1 MHz and then the pulses were coupled to the high-power fibre amplifier. The final amplifier consisting of a ~3 m-long active fibre with a core diameter of 25 μm was pumped by the 10-W laser diode, which allowed us to produce the picosecond pulses with energy up to 1 μJ at the output. After amplification and compression the pulse duration was 300 fs.

6. Conclusions

The ophthalmology laser system presented in paper was based on the all-fibre femtosecond laser working at $\lambda = 1067$ nm with a pulse duration less than 400 fs. The repetition rate of laser pulses was changed from 200 kHz to 1 MHz. Small aberration objectives were used for focusing the laser beam with a ~1 μJ pulse energy to a spot of size of several microns to ensure an optical breakdown. Different optical schemes were tested with the focal length of objectives in the range from 2 to 40 mm and the numerical aperture NA = 0.2–0.65. The focal point of the optical system could be adjusted to the depth up to 1 mm from the surface of the tissue. Glass, PMMA and agarose gels were used as a cornea tissue phantom during laboratory tests. Cutting procedure was performed with the speed up to 5 m s^{-1}. Clinical tests were successfully performed using our femtosecond laser system. Both eyes of a pig and human eyes were treated. The duration of the flap cornea creation was less than 20 s.

Also the paper describes the all-normal dispersion all-fibre laser ($\lambda = 1067$ nm) generating ultrashort pulses. The chirped picosecond pulse at the output of the oscillator was dechirped up to 140 fs close to the transform-limited pulse duration. To our knowledge, we used for the first time the combination of polarisation maintaining and nonpolarisation maintaining fibres in the fibre ring cavity to keep both the stable polarisation state and the passive mode-locking. To realise self-starting passive mode-locking in all-fibre cavity configuration, the film composite SWNT-CMC was used as a saturable absorber. The arrangement of the film saturable absorber on the surface of a side-polished fibre allows improving the optical resistance of the modulator and prolongs its operation time under conditions of interaction with high-intensity radiation. As a result of influence of nonlinear effects at passing of a pulse through the active fibre of the amplifier, the pulse duration increased up to 300 fs at its output energy of 1 μJ.

Acknowledgements. The authors are deeply grateful to A.S. Lobach from IPCP of the Russian Academy of Science (Chernogolovka) for the given materials and extremely grateful to the colleagues from 'IRE-Polus' (Fryazino) for their help. The authors also express their sincere gratitude to T.V. Malinsky for the invaluable help in experiments and useful discussions.

References

1. Neimz M.H. *Laser-Tissue Interactions: Fundamentals and Applications* (Berlin: Springer, 2007).
2. Ripken T., Bernau W., Oberheide U., Schumacher S., Knorz M., Kermani O., Lubatschowski H. *Proc. 19th Congress of German Ophthalmic Surgeons (DOC)* (Nuremberg, Germany, 2006).
3. Giguère D., Olivié G., Vidal F., Toetsch S., Girard G., Ozaki T., Kieffer J.C., Nada O., Brunette I. *J. Opt. Soc. Am. A*, **24** (6), 1562 (2007).
4. Chen Y.C., Raravikar N.R., Schadler L.S., Ajayan P.M., Zhao Y.-P., Lu T.-M., Wang G.-C., Zhang X.-C. *Appl. Phys. Lett*., **81**, 975 (2002).
5. Set S.Y., Yaguchi H., Tanaka Y., Jablonski M., Sakakibara Y., Rozhin A., Tokumoto M., Kataura H., Achiba Y., Kikuchi K. *Proc. Optical Fiber Communication Conf*. (Atlanta, GA, 2003).
6. Yamashita S., Inoue Y., Maruyama S., Murakami Y., Yaguchi H., Jablonski M., Set S.Y. *Opt. Lett*., **29**, 1581 (2004).
7. Garnov S.V., Solokhin S.A., Obraztsova E.D., Lobach A.S., Obraztsov P.A., Chernov A.I., Bukin V.V., Sirotkin A.A., Zagumennyi Y.D., Zavartsev Y.D., Kutovoi S.A., Shcherbakov I.A. *Laser Phys. Lett*., **4**, 648 (2007).
8. Kelleher E.J.R., Travers J.C., Sun Z., Rozhin A.G., Ferrari A.C., Popov S.V., Taylor J.R. *Appl. Phys. Lett*., **95**, 111108 (2009).
9. Wang J., Chen Y., Blau W.J. *J. Mater. Chem*., **19**, 7425 (2009).
10. Kataura H., Kamazawa Y., Maniwa Y., Umezu I., Suzuki S., Ohtsuka Y., Achiba Y. *Synth. Met*., **103**, 2555 (1999).
11. Nikolaev P., Bronikowski M., Bradley R., Rohmund F., Colbert D., Smith K., Smalley R. *Chem. Phys. Lett*., **313**, 91 (1999).
12. Kitiyanan B., Alvarez W.E., Harwell J.H., Resasco D.E. *Chem. Phys. Lett*., **317**, 497 (2000).
13. Okhotnikov O., Grudinin A., Pessa M. *New J. Phys*., **6**, 177 (2004).
14. Tausenev A.V., Obraztsova E.D., Lobach A.S., Chernov A.I., Konov V.I., Kryukov P.G., Dianov E.M. *Appl. Phys. Lett*., **92**, 171113 (2008).

15. Pepose J.S., Lubatschowski H. *Cataract and Refractive Surgery Today*, No. 10, 45 (2008).
16. Liu W., Kosareva O., Golubtsov I.S., Iwasaki A., Becker A., Kandidov V.P., Chin S.L. *Appl. Phys. B*, **76**, 215 (2003).
17. Nguyen N.T., Saliminia A., Liu W., Chin S.L., Vallée R. *Opt. Lett*., **28**, 1591 (2003).
18. Sun Q., Jiang H., Liu Y., Zhou Y., Yang H., Gong Q. *J. Opt. A: Pure Appl. Opt*., **7**, 655 (2005).
19. Khudyakov D.V., Lobach A.S., Obraztsova E.D., Nadtochenko V.A. *Khim. Vys. Energ*., **43** (4), 364 (2009) [*High Energy Chem*., **43** (4), 312 (2009)].